energies

MDPI

Article

Thermodynamic Comparison of the Steam Ejectors Integrated at Different Locations in Cogeneration Systems

Shifei Zhao *,†, Chunlan Wang †, Fan Duan and Ze Tian

School of Energy and Power Engineering, North China University of Water Resources and Electric Power, Zhengzhou 450045, China; wangchunlan@ncwu.edu.cn (C.W.); z20231191179@stu.ncwu.edu.cn (Z.T.)

* Correspondence: zhaoshifei@ncwu.edu.cn; Tel.: +86-1314-016-9687

† These authors contributed equally to this work.

Abstract: Under the challenge of global energy transition, coal-fired cogeneration systems are undergoing a technical revolution towards enhanced efficiency, heating capacity, and flexibility. In this paper, four schemes using a steam ejector integrated into a cogeneration system are designed. Considering operational safety, integrated locations are selected at the front and back of high- and medium-pressure turbines. Subsequently, the thermodynamic and operational characteristics under both design and off-design conditions are analyzed based on a model built in EBSILON Professional. Finally, a sensitivity analysis of the heating process is conducted. The results show that the integration of steam ejectors can increase the waste heat recovery ratio of exhaust steam by 18.42–45.61% under design conditions. The largest waste heat recovery ratio is obtained in System 4, resulting in the power generation efficiency (η_g) and gross energy utilization efficiency (η_p) of 81.95% and 65.53%, respectively. Meanwhile, the steam ejector can expand the power-load regulation range of the cogeneration system, and System 4 has the lowest lower power limit among all the systems. The η_p values of Systems 1–4 reach extreme values at different mixed steam pressures of the ejector. Increasing the pinch point temperature difference reduces the power load η_g and η_p of Systems 1–4. The results provide technical solutions for improving the heating capacity and efficient and flexible operation of cogeneration systems.

Keywords: waste heat recovery; cogeneration system; steam ejector; thermodynamic performance; sensitivity analysis

check for updates

Citation: Zhao, S.; Wang, C.; Duan, F.; Tian, Z. Thermodynamic Comparison of the Steam Ejectors Integrated at Different Locations in Cogeneration Systems. *Energies* **2024**, *17*, 2463. https://doi.org/10.3390/en17112463

Academic Editor: Carlo Roselli

Received: 17 April 2024
Revised: 5 May 2024
Accepted: 17 May 2024
Published: 22 May 2024

Copyright: © 2024 by the authors. Licensee MDPI, Basel, Switzerland. This article is an open access article distributed under the terms and conditions of the Creative Commons Attribution (CC BY) license (https://creativecommons.org/licenses/by/4.0/).

1. Introduction

Low-carbon energy systems are crucial for global energy transition to address the climate and energy crisis [1]. According to an International Energy Agency (IEA) report, coal remains the primary energy source for global energy systems [2,3]. Power from coal accounts for over 60% of China's power generation and over 70% in India. Recently, the European Union has either restarted or delayed the operation of some coal-fired power plants owing to international circumstances. Meanwhile, coal-fired power generation in the US has decreased, but it still accounts for approximately 20% of the total power generation. Therefore, the development of low-carbon coal technologies is crucial for global energy systems [4].

In recent decades, cogeneration has been widely implemented as a low-carbon technology, owing to its thermal and environmental advantages [5]. Based on energy cascade utilization, the overall efficiency of the traditional coal-fired cogeneration system can reach 70–80% [6]. The main challenges of coal-fired cogeneration systems are as follows. (1) Irreversible exhaust steam loss: for operational safety, traditional cogeneration systems must retain some steam to cool the turbine blades, resulting in a large and irreversible exhaust steam loss [7]. (2) A narrow regulation range of the power load: the rapid increase in renewable energy has a significant effect on the supply-side composition and stability of the

power grid [8]. However, owing to the coupling of heat and power, cogeneration systems frequently have a narrower power regulation range than power-only systems [9]. Therefore, increasing the operational flexibility of the existing coal-fired cogeneration systems would increase the share of renewable energy and reduce the energy storage and conversion devices like metal-ion batteries [10,11]. (3) Improvement of the heat capacity. Additionally, cogeneration systems are expected to have a higher heat capacity to replace heat-only boilers and achieve lower carbon emissions [12]. Consequently, more efficient and flexible cogeneration technologies with higher heating capacities are essential for innovations in coal-based energy technologies.

Although affected by economic and technical factors, waste heat recovery is a promising mechanism for technological upgrades in cogeneration systems [13,14]. On one hand, it can significantly reduce fuel consumption and increase heating capacity [15]. Driven by the thermal energy or electric power, the heat pump is commonly used in the waste heat recovery below 100 °C [16]. When the heat source temperature is in the range of 60–160 °C, the absorption heat pump (AHP) shows effective performance with the maximum energy and exergy production [17]. Integrated with the organic Rankine cycle (ORC) and AHP, the thermal efficiency of the cogeneration system could be improved by 9.38% [18]. Waste heat recovery with the high back-pressure technology could also significantly improve the heating capacity of the system [19,20]. On the other hand, waste heat recovery can improve the operational characteristics of cogeneration systems [21]. It has been proved that both the EHP and AHP had good application prospects in the flexibility enhancement of the cogeneration system [22]. And the utilization of heat pumps to recover waste heat can extend the feasible operating region of a cogeneration system and reduce the load rate by 10% [23].

Because it is simple and inexpensive compared with the above technologies, a steam ejector is also an alternative method of recovering waste heat [24]. In the steam ejector, high-pressure steam (driven steam) passes through a nozzle to generate a high-speed flow and a low-pressure zone. The low-pressure zone extracts low-pressure steam from outside and mixes it with the original steam. Subsequently, the mixed steam reaches the required medium pressure in the diffuser [25]. With a simple structure and nonpower-driven characteristics, steam ejectors are commonly used to provide heating, cooling, or refrigeration [26,27]. Steam ejectors also can improve both the thermodynamic performance and flexibility of cogeneration systems. A optimized steam ejector could increase the exergy efficiency by 6.1% of a cogeneration system [28]. And after the system integration, the peak load regulating capacity could increase by 94.80 MW for a 330 MW unit [29]. Steam ejectors are also highly compatible with various cogeneration technologies. Chen et al. [30] used a steam ejector to produce steam for an AHP, resulting in a low electricity cost of 0.0329 USD/kWh. Cao et al. [31] proposed a cogeneration system integrated with an ORC and a steam ejector, the thermal efficiency of which reached 79.0%. Fazali et al. [32] observed that the exergy efficiency of an integrated system, including gas turbine, ORC, and ejector could reach 40.76%. Zhang et al. [33] designed a novel cascade system based on a steam ejector and high-back-pressure technology, and the heating capacity increased by 4.21%.

The abovementioned studies analyzed the advantages of waste heat recovery using steam ejectors in a cogeneration system. However, various steam sources are available for the driven steam of steam ejectors in coal-fired cogeneration systems. The choice of the driving steam source has a significant impact on the thermodynamic and operational characteristics of the entire system. In addition, the performance of a system is significantly affected by the selection of the key parameters in the heat transfer process. Currently, these effects have not been analyzed or discussed.

In this paper, four options for integrating steam ejectors at different locations in the cogeneration system are designed. Based on the energy level from low to high, the sources of the driven steam are selected from the outlets of the medium-pressure turbine (MPT) and high-pressure turbine (HPT), the inlet of the MPT, and the main steam. Subsequently,

the thermodynamic and operational characteristics under both design and off-design conditions are compared. Furthermore, a sensitivity analysis of the key parameters is performed to determine their influence on the thermodynamic performance.

2. System Description

In this paper, a typical 300 MW sub-critical coal-fired cogeneration power plant in Northern China is selected as the basic system (BS). In Section 2.1, the main parameters of the basic system are introduced. After the primary energy flow analysis of the basic system, four options for integrating steam ejectors at different locations in the cogeneration system are described in Section 2.2.

2.1. Traditional Coal-Fired Cogeneration System (Basic System)

A schematic of the basic system is shown in Figure 1. The power component of the system consists of three turbine cylinders: an HPT, MPT, and low-pressure turbine (LPT). The exhaust steam is condensed in the condenser and sent to the boiler through a regenerative system consisting of three low-pressure regenerative heaters (RHs), one deaerator, and three high-pressure RHs. The steam used for heating is extracted between the MPT and LPT. The pressure of the heating steam is maintained at or above 0.4 MPa to ensure an adequate temperature difference between steam and water in the heat exchanger (HE). This enables the hot-water outlet temperature to satisfy the district heating (DH) requirements. The main parameters under the turbine maximum continuous rating (TMCR) and maximum heating conditions of the basic system are listed in Table 1. Table 2 gives the main parameters of the regenerative system under the THA condition. All the data are collected from the design book of the turbine.

Table 1. Main parameters of the basic system.

Items	Unit	TMCR	Maximum Heating (Design)
Main steam			
Mass flow rate	t/h	1017.92	1017.92
Pressure	MPa	16.67	16.67
Temperature	°C	538	538
Reheated steam			
Mass flow rate	t/h	847.02	839.05
Pressure	MPa	3.58	3.48
Temperature	°C	538	538
Extraction steam for heating			
Mass flow rate	t/h	–	500
Pressure	MPa	–	0.4
Steam temperature	°C	–	244.28
Drain water temperature	°C	–	104
Heat load	MW	–	428.97
Power load	MW	322	245.47
Net power load	MW	313.42	237.19
Energy input	MW	797.42	797.42
Back pressure	kPa	14	14

Table 2. Main parameters of the regenerative system under the THA condition.

Items	Unit	RH1	RH2	RH3	Deaerator	RH5	RH6	RH7
Pressure	MPa	6.20	3.98	1.90	1.03	0.63	0.26	0.089
Temperature	°C	390.4	332.6	442.7	355.9	294.5	–	–
Enthalpy	kJ/kg	3151.5	3051.3	3343.3	3170.5	3049.9	2868.2	2677.8
Mass flow	t/h	69.41	60.00	33.66	29.60	43.69	41.50	47.60

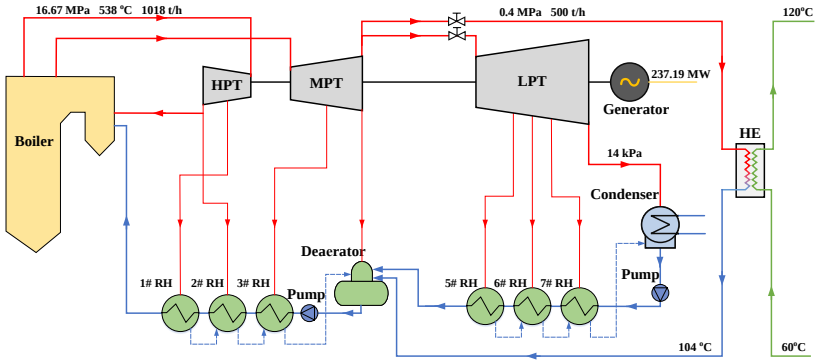

Figure 1. Schematic of the coal-fired cogeneration system (basic system).

The Sankey diagram in Figure 2 shows the energy flow in the basic system. The power grid and DH system utilize 74.66% of the input energy, with 44.48% consumed by the DH system. The energy from the heating steam accounts for 52.19% of the total energy. This can significantly decrease the steam to the LPT and reduce exhaust steam loss. Subsequently, 7.71% of the total energy after the HE enters the regenerative system in the form of feedwater. Such cascade utilization of energy is the primary energy-saving mechanism of traditional cogeneration systems. However, in the DH network heater, the energy on the hot side primarily results from the latent heat of the heating steam condensation process, whereas the cold side is a nonphase-change process, resulting in a temperature increase. Therefore, the DH network heater is associated with significant irreversible exergy loss, which is consistent with the second law of thermodynamics. Meanwhile, a specific amount of steam must be retained to cool the blades for the safe operation of the LPT [34]. Thus, the loss of exhausted steam still accounts for 18.02% in the basic system even under maximum heating conditions.

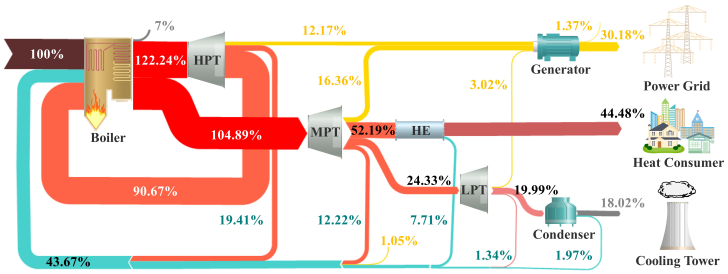

Figure 2. Energy flow of the basic system.

2.2. Cogeneration System Integrated with the Steam Ejector

For these reasons, a cogeneration system integrated with a steam ejector is suggested as shown in Figure 3. The steam ejector enables the driven steam to pass through a nozzle to create a low-pressure zone. Low-pressure steam is then extracted to produce medium-pressure steam. Consequently, the steam ejector recovers low-grade steam heat and controls the steam pressure levels. In this system, the driven and low-pressure steam of the ejector are the heating and exhaust steam, respectively. Additionally, the mixed steam from the ejector serves as the primary heat source for the returned water. After preheating in the first HE, the water is further heated in the second HE by the heating steam to attain the required temperature for the DH network.

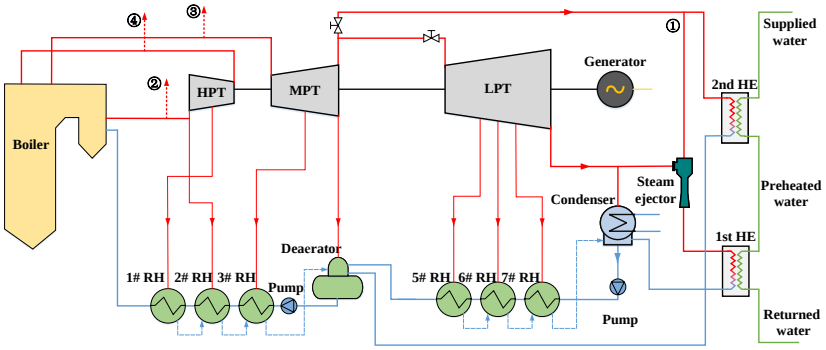

Figure 3. Schematic of the cogeneration system integrated with the steam ejector.

Compared with the basic system, the following are the key benefits of the new system: (1) Recovery of waste heat from exhaust steam—the waste heat recovery of the exhaust steam can directly reduce the loss in the condenser, which accounts for 18.02% of the basic system. Although it has a slight impact on power generation, it can significantly increase the heat load of the system. Thus, the performance of the system can be improved by reducing gross loss. (2) Reduction in exergy loss in DH network heater: In the basic system, the heating steam is selected as the only heat source for the HE. The large mean temperature difference between steam and water results in a large exergy loss in the HE. The novel system uses a cascade heating process that employs low-grade steam (from the steam ejector) as the first-stage heat source and high-grade steam (from the heating steam) as the second-stage heat source. As a result of the optimization, the system exhibits a reduction in exergy loss compared with the basic system.

In addition to the above process, the steam driven by the ejector can be another source. In this study, the driven steam is extracted before and after each turbine. This is because the mass flow of the driven steam is large. If the driven steam is extracted from the inside of the turbine, a larger mass flow difference can result between the front and rear sides of the turbine. This is detrimental to operational stability and safety. Driven steam is listed based on the energy levels, ordered from low to high, as follows: Point 1: Steam between the MPT and LPT. Point 2: Steam after the HPT. Point 3: Steam before the MPT. Point 4: Steam before the HPT. These systems are identified asSystems 1 to 4, respectively. As shown in Figure 3, these four systems utilize the outlet steam from the steam ejectors as the first-stage heat source, whereas the steam extracted between the MPT and LPT is the second-stage heat source. All these systems share the same constraints on the mass flow rate of the main and exhausted steam as the reference system.

3. Calculation Model and Evaluation Method

In this section, the modeling software and assumptions are first introduced in Section 3.1. The evaluation methods of the overall performance and heating process are presented in Section 3.2, which are based on the first law of thermodynamics and the second law of thermodynamics, respectively.

3.1. Calculation Model

In this study, EBSILON professional (version 16.02, Iqony Solutions GmbH, Essen, Germany) is selected as the model platform, as it is widely used in energy system simulations and has been proven to be precise in many studies [35]. The following assumptions are adopted: (1) The operational mode of the boiler (steam generator) is a modified sliding pressure operation according to the design book. (2) The condenser pressure, temperature differences of RHs, pump efficiencies, and pressure loss ratios of the pipes remain unchanged in the off-design conditions. (3) The inlet steam pressure of the LPT is 0.4 MPa or higher with different steam mass flow rates. (4) The boiler efficiency (η_b) and generator efficiency (η_{gen}) are 93% and 98.85%, respectively. (5) The turbine mechanical and heat

losses are disregarded, and the off-design calculations follow Stodola's cone law. Figure 4 shows the System 4 model constructed using EBSILON Professional.

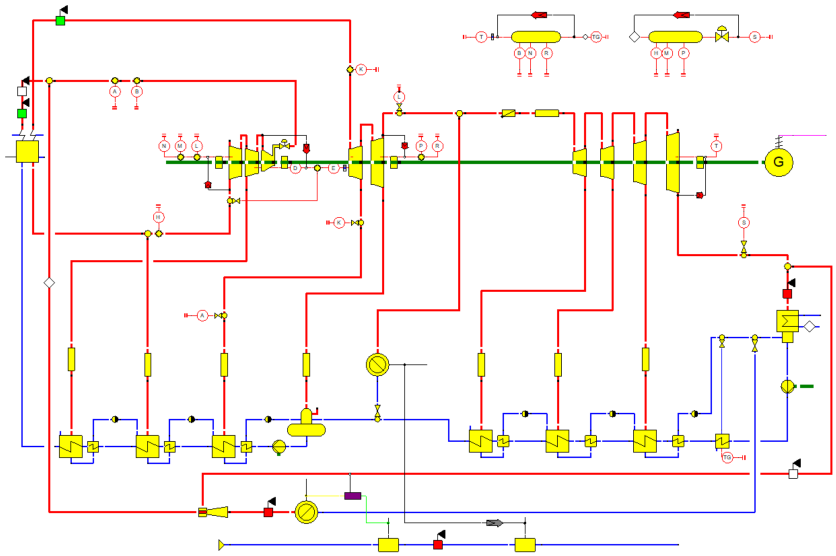

Figure 4. Schematic of the model in EBSILON Professional (System 4).

The heat consumption of the boiler Q_b can be calculated as

$$Q_b = [m_s(h_s - h_g) + m_r(h_{r,out} - h_{r,in})]/\eta_b \quad (1)$$

where m_s and m_r are the mass flow rates of the main and reheated steam, respectively (kg/s). h_s, h_g, $h_{r,in}$, and $h_{r,out}$ are the specific enthalpies of the main steam, given water, and the inlet and outlet of the reheat steam, respectively (kJ/kg).

The power output of each turbine stage P_s is expressed as

$$P_s = m_{in}(h_{in} - h_{out,is})\eta_{is} \quad (2)$$

where m_{in} is the mass flow rate of the inlet steam (kg/s). h_{in} and $h_{out,is}$ are the specific enthalpies of the inlet and outlet steam in the isentropic process, respectively (kJ/kg). η_{is} is the isentropic efficiency (%).

The gross electric power P_g is derived as

$$P_g = \sum_{i=1}^{n} P_s \eta_{gen} \quad (3)$$

Based on the above assumptions and the model platform, Figure 5 provides a comparison between the simulated results and the values given in the design book of the turbine. The power-only conditions included the TMCR, turbine heat acceptance (THA), 75% THA, 50% THA, and 40% THA. The maximum relative error (RE) was −0.39% in the 75% THA condition. This demonstrates the high precision of the model used in this study.

The detailed process of the cascade heating system is shown in Figure 6. The performance of a steam ejector is typically evaluated using the compression ratio (β), expansion ratio (σ), and ejector coefficient (μ), which are expressed as [36]

$$\beta = \frac{p_3}{p_2} \quad (4)$$

$$\sigma = \frac{p_1}{p_2} \quad (5)$$

$$\mu = \frac{m_2}{m_1} \tag{6}$$

where p_1, p_2, and p_3 are the pressures of the driven, exhaust, and mixed steams in the ejector, respectively (MPa); and m_1 and m_2 are the mass flow rates of the driven and exhaust steam, respectively (kg/s).

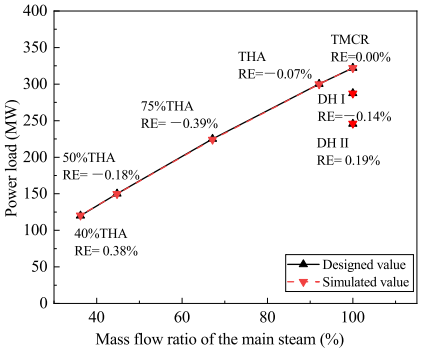

Figure 5. Comparison between simulated and designed values.

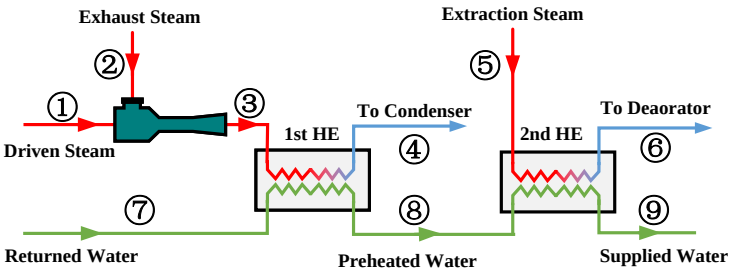

Figure 6. Diagram of the cascade heating system.

The heat loads of the first and second stages of the heating process are given by

$$Q_{1st} = m_3h_3 - m_4h_4 = m_8h_8 - m_7h_7 \tag{7}$$

$$Q_{2nd} = m_5h_5 - m_6h_6 = m_9h_9 - m_8h_8 \tag{8}$$

where m_3, m_4, m_5, m_6, m_7, m_8, and m_9 are the mass flow rates of the mixed steam of the ejector, drain to condenser, heating steam, drain to deaerator, returned, preheated, and supplied water, respectively, (kg/s). Additionally, h_3, h_4, h_5, and h_6 denote the enthalpies of the corresponding steam and water, respectively (kJ/kg).

Subsequently, the gross heat load Q_g can be derived as

$$Q_g = Q_{1st} + Q_{2nd} \tag{9}$$

The heat load ratio of the first stage (δ), heated by the ejector outlet steam, can be expressed as follows:

$$\delta = \frac{Q_{1st}}{Q_g} \times 100\% \tag{10}$$

3.2. Evaluation Method

Except for the performance indicators of the ejector shown in Equations (4)–(6), the overall performance and heating process are also evaluated. The overall performance indicators are based on the first law of thermodynamics, which includes gross energy utilization efficiency η_g and power generation efficiency η_p. These indicators are given as follows [37]:

$$\eta_g = \frac{Q_g + P_g}{Q_b} \times 100\% \tag{11}$$

$$\eta_p = \frac{P_g}{Q_b - Q_g/\eta_b} \times 100\% \tag{12}$$

The performance indicators of the heating process, energy quality coefficient (λ), and exergy efficiency (Ψ_{ex}), are based on the second law of thermodynamics [38]. λ represents the ratio of maximum useful work (exergy, E_s) to total energy input (Q_s). For steam, λ_s can be calculated as follows:

$$\lambda_s = \frac{E_s}{Q_s} \tag{13}$$

where T_0 and T_s are the ambient and saturated-steam temperatures, respectively (K).

The energy quality coefficient of water (λ_w) is given by

$$\lambda_w = 1 - \frac{T_0}{T_{out} - T_{in}} \ln \frac{T_{out}}{T_{in}} \tag{14}$$

where T_{out} and T_{in} are the inlet and outlet water temperatures, respectively, (K).

Subsequently, the exergy efficiency of the heating process Ψ_{ex} is derived as follows:

$$\Psi_{ex} = \frac{\lambda_w}{\lambda_s} \times 100\% \tag{15}$$

4. Result and Discussion

In this section, the overall thermodynamic performance and the heating process analysis under the design condition are first evaluated in Sections 4.1 and 4.2. Then, the thermodynamic and operational performance under the off-design conditions are conducted in Section 4.3. In Section 4.4, the influence of two key parameters on the heating process and overall performance is analyzed. Finally, Section 4.5 gives the discussion of the above results.

4.1. Thermodynamic Performance under the Design Condition

Drive steam quality has a significant impact on the system performance. On one hand, the higher drive steam quality leads to greater power load decrement. On the other hand, it could also recover more waste heat from exhaust steam, resulting in higher heating capacity. Meanwhile, driven steam in System 3 has a lower steam pressure but a higher temperature than that in System 2. Therefor, detailed energy flow diagrams are needed to show the energy distribution within these systems, shown in Figure 7. The results indicate that as the driven steam quality of the steam ejector increases, P_g decreases. However, both the mass flow rate of the recovered steam and Q_g improve. Specifically, the proportion of P_g decreases from 30.37% to 28.33%, 27.78%, and 26.35%, with decreases of 1.04%, 2.59%, and 4.02%, respectively. The proportion of Q_g increases by 5.08%, 6.60%, and 8.86%, respectively. Moreover, the heat recovery ratios of the exhaust steam are 18.42%, 35.93%, 37.23%, and 45.61%. This can decrease exhaust steam loss from 15.52% to 12.51%, 12.05%, and 10.73%, respectively.

Figure 8 shows the comprehensive distributions of P_g, Q_g, and the losses of the five systems under the design conditions. As the driven steam quality of the ejector increases, P_g and the energy loss decrease as Q_g increases. The losses decrease from 199.13 MW in the basic system to 142.08 MW, reflecting a decrease of 57.05 MW. P_g decreases from 237.19 MW to 207.50 MW, with a decrease of 29.69 MW, whereas Q_g increases from 349.52 to 437.77 MW, with an increase of 88.25 MW. Note that the difference in losses and P_g between System 2 and System 3 is minor, at 0.16 and 3.17 MW, respectively, but the difference in heat supply between them is significant, at 21.64 MW. This is because the driving steam pressures of the two systems are similar and the reheating process of the driven steam has minimal influence on P_g.

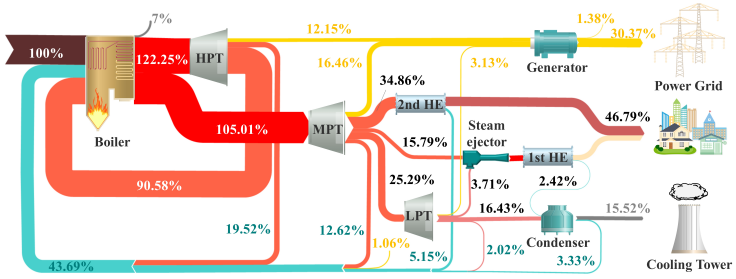

(**a**)

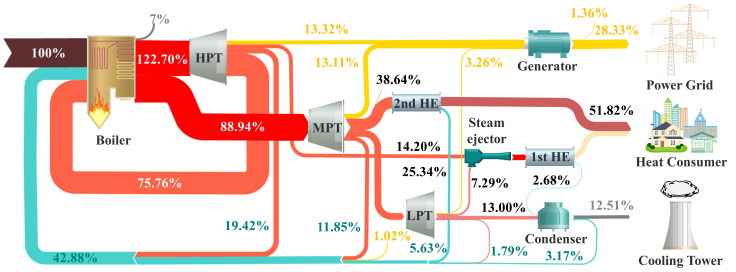

(**b**)

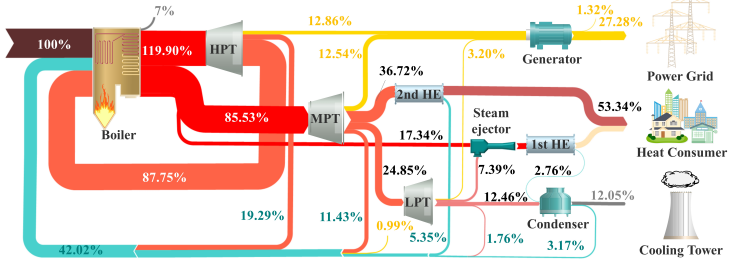

(**c**)

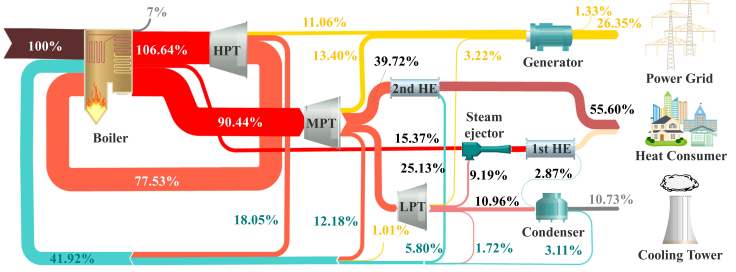

(**d**)

Figure 7. Energy flow of the novel system: (**a**) System 1; (**b**) System 2; (**c**) System 3; (**d**) System 4.

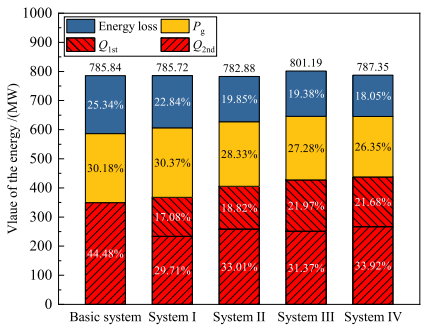

Figure 8. Energy distribution of the five systems under the design conditions.

Figure 9 presents a comparison of the η_g and η_p values for the five systems. As the quality of the driving steam improves, η_g gradually increases from 74.66% to 81.95%, representing an increase of 7.29%. The corresponding η_p also exhibits an upward trend, increasing from 57.85% to 65.53% in increments of 7.68%. Notably, Systems 2 and 3 share the same η_p, both at 63.98%.

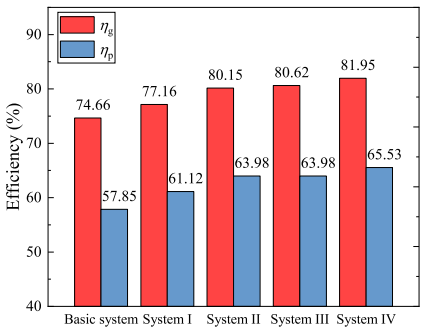

Figure 9. Efficiencies of the five systems under the design conditions.

4.2. Heating Process Analysis under the Design Conditions

The integration of the steam ejector can change the performance of the heating process, not only Q_g but also the thermodynamic characteristics. Figure 10 shows a comparison of the T-Q diagrams of the five systems. The Q_g values of the systems with steam ejectors are higher than those of the basic system. As the quality of the driven steam improves, Q_g successively increases by 18.12, 56.19, 77.83, and 88.25 MW in Systems 1–4, respectively. Additionally, in the low-temperature range (60–80 °C) of the first-stage heating process, the temperature difference is reduced significantly compared with the reference system. However, owing to the high superheat of the steam, exergy losses of the heat release process of the superheated steam are large, particularly for Systems 3 and 4. In the second stage, although the heat release processes are similar, the average temperature of the cold source (DH network water) is higher in Systems 1–4 than that in the basic system, which can also reduce the exergy loss.

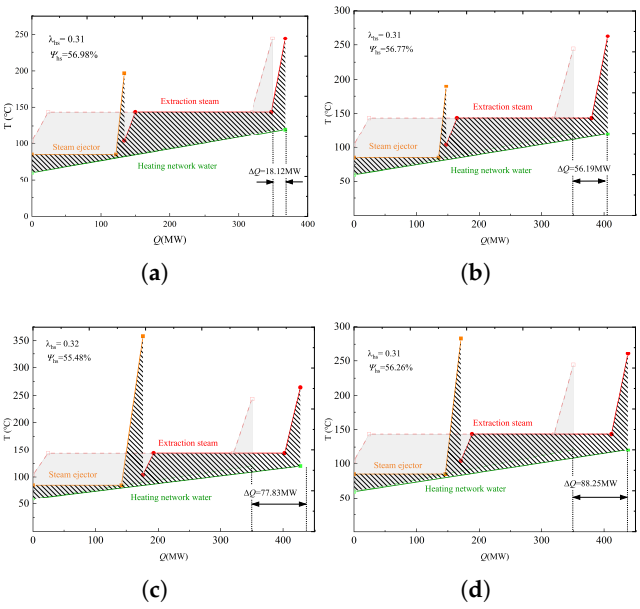

Figure 10. T-*Q* diagrams of the heating process in the five systems: (**a**) System 1; (**b**) System 2; (**c**) System 3; (**d**) System 4.

Table 3 compares the thermodynamic performance indices of all systems. $\lambda_{s,2nd}$ is similar for Systems 1–4, but $\lambda_{s,1st}$ is relatively low. Consequently, the $\lambda_{s,1st}$ values of systems

with a steam ejector are lower than those of the basic system. Among the novel systems, System 3 has the highest values of both $\lambda_{s,1st}$ (0.275) and λ_s (0.350), resulting in the lowest Q_g (55.48%). Nonetheless, Ψ_{ex} of System 3 is still 4.60% higher than that of the basic system.

Table 3. Comparison of thermodynamic performance results of the heating process.

Items	Basic System	System 1	System 2	System 3	System 4
$\lambda_{s,1st}$		0.246	0.245	0.275	0.260
$\lambda_{s,2nd}$	0.348	0.348	0.350	0.350	0.350
λ_s	0.348	0.311	0.312	0.319	0.315
λ_w	0.177	0.177	0.177	0.177	0.177
Ψ_{ex}	50.88%	56.98%	56.77%	55.48%	56.26%

Table 4 presents a performance comparison of the steam ejectors in Systems 1–4. System 4 recovers the most energy from exhausted steam, which is 72.34 MW, 43.18 MW higher than that of System 1. Meanwhile, μ of System 4 is the highest, reaching 0.78. The trend of μ follows that of σ. Although System 3 has a higher steam quality than System 2, the pressure loss during reheating results in a smaller σ for System 3 than that for System 2, resulting in a lower μ. Among Systems 1–4, System 3 has the highest heating ratio and driving steam energy, reaching 41.19% and 138.92 MW, respectively.

Table 4. Performance of steam ejectors in Systems 1–4.

Items	Unit	System 1	System 2	System 3	System 4
Extraction steam	MW	124.09	111.20	138.92	120.98
Exhaust steam	MW	29.16	57.07	59.20	72.34
Return water	MW	18.99	20.96	22.06	22.62
Compression ratio (β)	%	4.13	4.13	4.13	4.13
Expansion ratio (σ)	%	28.57	234.40	207.95	1190.71
Ejector coefficient (μ)	%	0.27	0.60	0.58	0.78
δ	%	36.51%	36.31%	41.19%	38.99%

4.3. Thermodynamic and Operational Performance under the Off-Design Conditions

Considering that the system does not always operate with the maximum flow rate, the performance with different main-steam mass flow ratios is also conducted, shown in Figure 11. When the ratio decreases from 100% to 40%, System 4 has the largest reduction in Q_g, with a decrement of 350.95 MW, whereas the corresponding reduction in P_g is the lowest at 105.67 MW. In contrast, the reduction in Q_g for the basic system is the lowest at 278.43 MW. The reduction in P_g for the basic system is the largest at 130.54 MW. This can result in efficiency changes as shown in Figure 10b. With a decrease in the mass flow ratio, η_g and η_p of the five systems exhibit similar trends. This is because the flow rate of the exhaust steam remains constant under different conditions, resulting in a slight change in the exhaust steam loss. When the mass flow ratio decreases from 100% to 40%, the decrements in η_g range from 23.96% to 28.32%, whereas those of η_p range from 18.85% to 26.12%. Despite the largest decrease, η_g and η_p of System 4 remain the highest under different mass flow ratios.

Meanwhile, as the main steam flow ratio decreases, the heating ratio of the steam ejector increases slightly in Systems 1–4 as shown in Figure 10c. System 1 experiences the largest increase of 1.93%, from 56.99% to 55.06%. The heat load ratios of the steam ejector (δ) in Systems 2 and 4 change slightly as the flow ratio decreases from 100% to 70%, but exhibit a significant increase as it further decreases to 40%. The Ψ_{ex} values of all four systems exhibit a decreasing trend, which is primarily attributed to the increase in the energy levels of the extraction steam and steam ejector as shown in Figure 10d. Furthermore, we can infer that the impact of the flow ratio changes on Ψ_{ex} is insignificant. System 1 experiences the most significant change in Ψ_{ex} among Systems 1–4, with a decrease of 2.69% when the flow ratio decreases from 100% to 40%.

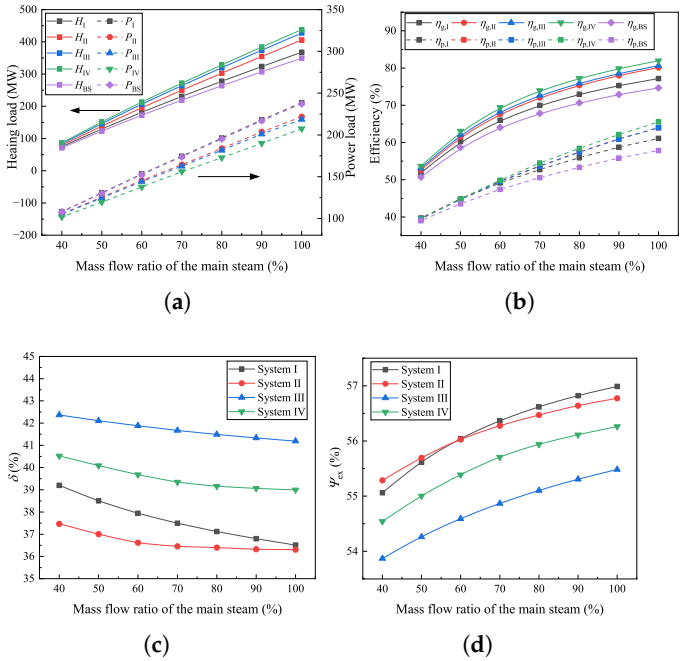

Figure 11. Thermodynamic performance with different main steam mass flow ratios: (**a**) Heat and power loads; (**b**) Efficiency; (**c**) Heat load ratio of the first stage; (**d**) exergy efficiency.

Figure 12 shows the heat–power load operational regions of the five systems. At the same heat load, the upper and lower power limits of System 1 are slightly wider than those of the basic system. The upper power limits of Systems 2 and 3 remain relatively unchanged; however, the lower power limits are significantly lower than those of the basic system. Although the upper power load limit of System 4 is slightly lower than that of the basic system, its lower power load limit is lower than those of the other four systems.

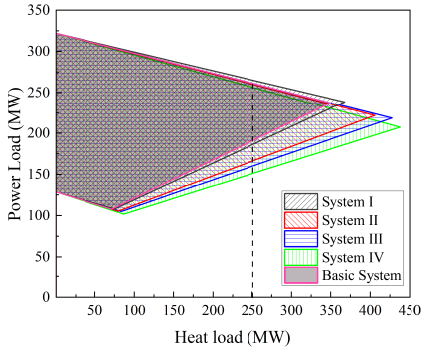

Figure 12. Heat–power loads operational region of the five systems.

With the constant heat load of 250 MW, Figure 13 gives the changes of η_g and η_p at different heat loads. η_g and η_p of all systems are increased with the decrement in the power load. The reason is that with the constant heat supply, the decreasing in power load is regulated by the reduction in the main steam flow. It could also lead to the decrement in the exhaust steam loss. With the same power load, η_g and η_p of System 1 are higher than those of the basic system when η_g and η_p of Systems 2–4 are lower. Among them, η_g and η_p of System 4 are the lowest in the power range of 261.32–190.94 MW.

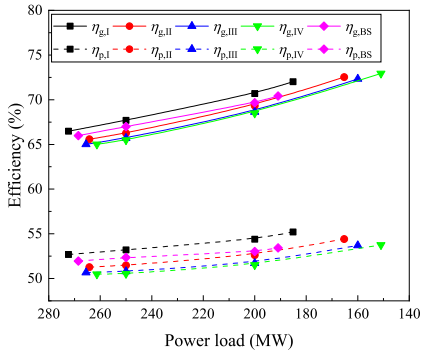

Figure 13. Efficiencies at different power loads (H = 250 MW).

The decrement in the lower power load limit could improve the regional share of renewable energy, which could provide peaking benefits to power plants. When the heat load is 250 MW, the lower power load limits of Systems 1–4 decrease by 4.79, 24.67, 30.96, and 39.97 MW, respectively, when compared with the basic system (190.94 MW). Assuming that the power is replaced by the renewal energy, the increasing powers would be 115.03, 592.12, 743.06, and 959.33 MWh per day with Systems 1–4, respectively. This would result in the standard coal consumption decrement of Systems 1–4 by 35.07, 180.52, 226.54, and 292.47 t, equivalent to the CO_2 emission reduction by 100.65, 518.11, 650.18, and 839.42 t, respectively [39]. Considering the peak-shaving policy, assuming that the subsidized price is 68 USD/MWh, the peaking revenue of Systems 1–4 would reach 7822, 40,264, 50,528, and 65,235 USD per day, respectively.

4.4. Sensitivity Analysis of the Heating Process

The heat load ratio of the steam ejector (δ) is directly affected by the temperature of the preheated water (T_P), which subsequently influences the thermodynamic performance of the system. The two key parameters that can affect T_P are the pressure of the mixed steam (p_M) and pinch-point temperature difference (ΔT_P) of the heating process. In this section, the influence of p_M and ΔT_P on the heating process and overall performance is analyzed.

As shown in Figure 14, an improvement in p_M can result in increases in T_P and β. As p_M increases from 40 to 90 kPa, T_P increases by 20.83 °C from 70.89 to 91.71 °C, whereas β increases by 3.57 from 2.86 to 6.43. Furthermore, the increment in β can reduce μ of the steam ejector as shown in Figure 14b. As p_M increases from 40 to 90 kPa, the mu values of Systems 1–4 exhibit similar trends, with decrements of 0.44–0.66. A higher pressure of the extracted steam results in a larger decrease in μ.

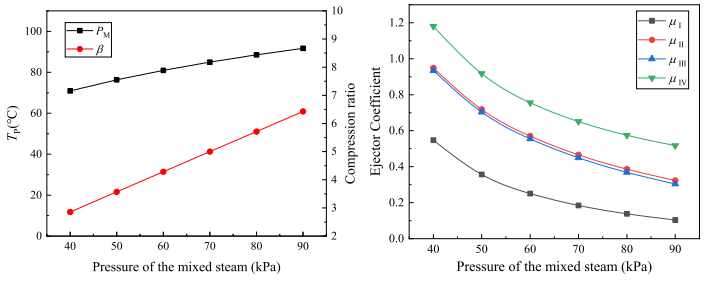

(**a**) (**b**)

Figure 14. Influence of P_M on the heating process: (**a**) T_P and compression ratio; (**b**) Ejector coefficient.

Figure 15 shows the effect of p_M on the performance of Systems 1–4. As p_M increases from 40 to 90 kPa, the trends in P_g and Q_g differ. Q_g of System 1 decreases from 370.22 to 350.35 MW, whereas P_g increases slightly from 237.84 to 239.56 MW. However, the P_g and Q_g values of other systems show the opposite trend to System 1, increasing by 19.76–86.04 MW and decreasing by 20.96–49.89 MW, respectively, as shown in Figure 15a. This results in

changes in η_g and η_{gen} as shown in Figure 14b. The maximum η_{gen} values of Systems 1–4 are 61.48%, 63.97%, 63.96%, and 66.08%, respectively. The corresponding p_M are 50, 60, 60, and 70 kPa, respectively. The η_g of System 4 is increased from 79.35% to 83.62%, whereas the maximum η_g of Systems 1–4 reach 77.45%, 80.19%, and 80.79%, respectively.

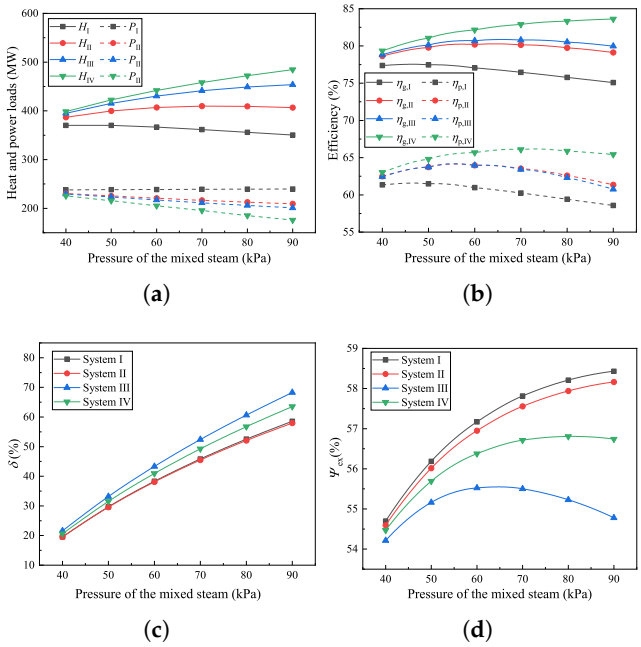

Figure 15. Influence of P_M on the thermodynamic performance: (**a**) Heat and power loads; (**b**) Efficiency; (**c**) Heat load ratio of the first stage; (**d**) exergy efficiency.

Meanwhile, as p_M increases from 40 to 90 kPa, δ increases significantly as shown in Figure 15c. The four systems have different increments ranging from 38.41% to 46.68%, with System 3 having the largest increment. Ψ_{ex} of Systems 1 and 2 exhibit an increasing trend when p_M increases from 40 to 90 kPa, which are increases of 3.73% and 3.57%, respectively. The maximum Ψ values of Systems 3 and 4 are 55.52% and 56.80%, with corresponding p_M values of 60 and 80 kPa, respectively.

Figure 16 shows the effect of ΔT_P on the performance results of Systems 1–4. As ΔT_P increases from 1 to 9 °C, the Q_g values of all systems exhibit a decreasing trend. System 1 experiences the smallest decrement of 7.64 MW, whereas System 4 experiences the largest decrement of 44.55 MW. Correspondingly, P_g of System 1 remains almost unchanged, whereas the P_g values of Systems 2–4 increase by 6.67, 8.74, and 15.05 MW, respectively. Additionally, an increase in ΔT_P causes a decrease in both η_g and η_{gen} for all systems. As ΔT_P increases from 1 to 9 °C, the η_g values of Systems 1–4 decrease by 1.05%, 2.47%, 2.78%, and 3.68%, whereas the η_{gen} values decrease by 1.44%, 3.29%, 3.51%, and 5.09%, respectively.

As ΔT_P increases from 1 to 9 °C, both heating ratios and Ψ_{ex} of all systems exhibit decreasing trends. The decrease in δ in System 3 is the largest at 16.62%, whereas that of System 2 is the smallest at 14.44%. Meanwhile, the Ψ_{ex} values of Systems 1–4 decrease slightly, decreasing by 1.98–2.74%.

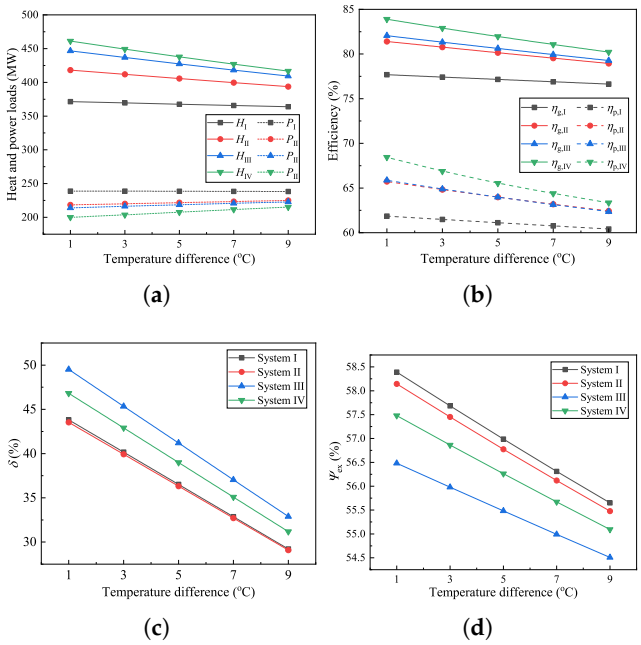

Figure 16. Influence of ΔT_P on the thermodynamic performance: (**a**) Heat and power loads; (**b**) Efficiency; (**c**) Heat load ratio of the first stage; (**d**) exergy efficiency.

4.5. Discussion

The above analysis shows that integrating steam injectors at different locations has different effects on the thermodynamic and operational characteristics of a system. From the thermodynamic analysis of the heating process, Systems 1 and 2 have higher exergy efficiencies, indicating that their heat transfer processes are more rational. However, System 4 is more advantageous in terms of efficiency in the maximum heat load, heat capacity, and lower power load limits. This is primarily caused by the difference in the quantity of recovered waste heat. Therefore, although this study reveals the potential of different integrated systems in terms of thermodynamic and operational characteristics, further improvement of the system is required. For example, the lower exergy efficiencies of the heat transfer process in Systems 3 and 4 are primarily caused by a high degree of superheating in the mixed steam of the ejector. The proper utilization of superheating aids in further improving system performance. In addition, the economic benefits of heat capacity and flexibility are highly influenced by the policies and development plans of the region; therefore, the results of this study must be combined with the actual loads and peaking policies of the region when they are used in practice. Our team will continue to conduct further studies.

5. Conclusions

In this study, coal-fired cogeneration systems integrated with steam ejectors at different locations are designed and modeled using EBSILON Professional. The thermodynamic and heating process analyses are performed under the design condition. Furthermore, the thermodynamic and operational characteristics of the five systems are compared under off-design conditions. Finally, sensitivity analyses are performed on the key parameters of the cascade-heating process.

Waste heat recovery using a steam ejector can significantly reduce exhaust steam loss in the cogeneration system. As the driving steam level increases, the heat recovery ratios of the exhaust steam under the design conditions are between 18.42% and 45.61% for Systems 1–4. Among them, System 4 has the most significant increase in Q_g, resulting in increases of 7.29% in η_g and 7.69% in η_p compared with the basic system.

As the main steam mass flow ratio decreases, P_g and Q_g, as well as η_g and η_p, for all systems have a decreasing trend. System 4 experiences the largest reduction in Q_g, whereas the corresponding reduction in P_g is the smallest among Systems 1–4. Although System 4 experiences the greatest decline, it still has the highest η_g and η_p values among the different flow ratios. The operational analysis indicates that using a steam ejector can expand the power-load regulation range of a cogeneration system, and System 4 has the lowest low-power limit among all systems. With the heat load of 250 MW, System 1 has the highest η_g and η_p in the power range of 261.32–190.94 MW.

T_P and the thermodynamic performance of the system are directly affected by p_M of the ejector and ΔT_P of the heating process. When p_M increases, μ and Q_g increase, whereas T_P and P_g decrease. The η_p values of Systems 1–4 reach extreme values at different P_M values. Increasing ΔT_P can cause a reduction in P_g, η_g, and η_p of Systems 1–4. Meanwhile, all systems exhibit a decreasing trend in their heating ratios and Ψ_{ex}.

In conclusion, with the increment of the driving steam energy level, the maximum power load is decreased. Meanwhile, the heat recovery ratios of the exhaust steam and heating capacity are enhanced, resulting in increases in η_g and η_p. From the operational regulation point of view, the increment in the drive steam energy level could reduce both the upper and lower power limits of the system, and the latter reduction is more significant. This provides insight for improving the deep peaking capability of the cogeneration systems. The result contributes to a higher percentage of renewable energy in the region. In the next research, the following research directions will be conducted based on the paper: (1) detailed analysis of the coal saving, carbon reduction and economic benefit considering the specific policies and regional plan; (2) optimization scheme to decrease the superheat of mixed steam in Systems 3 and 4.

Author Contributions: Conceptualization, S.Z. and C.W.; methodology, S.Z.; software, C.W. and F.D.; validation, C.W., Z.T. and F.D.; formal analysis, S.Z.; investigation, C.W.; resources, S.Z.; data curation, F.D.; writing—original draft preparation, S.Z. and C.W.; visualization, Z.T.; supervision, S.Z.; project administration, S.Z. and C.W.; funding acquisition, S.Z. All authors have read and agreed to the published version of the manuscript.

Funding: The financial support from the National Natural Science Foundation of China (Grant No. 52206012) and Project of Central Plains Science and Technology Innovation Leading Talents of Henan Province (Grant No. 224200510022) are gratefully acknowledged.

Data Availability Statement: The original contributions presented in the study are included in the article, further inquiries can be directed to the corresponding author.

Conflicts of Interest: The authors declare no conflicts of interest.

Abbreviations

The following abbreviations are used in this manuscript:

AHP	Absorption heat pump
BS	Basic system
DH	District heating
EHP	Electric heat pump
HE	Heat exchanger
HPT	High-pressure turbine
LPT	Low-pressure turbine
MPT	Medium-pressure turbine
ORC	Organic Rankine cycle
RE	Relative error
RH	Regenerative heater
THA	Turbine heat acceptance
TMCR	Turbine maximum continuous rating

References

1. Lu, D.; Peng, Y.; Sun, J. Dual-Stage Optimization Scheduling Model for a Grid-Connected Renewable Energy System with Hybrid Energy Storage. *Energies* **2024**, *17*, 737. [CrossRef]
2. *Coal 2022: Analysis and Forecast to 2025*; Technical Report; International Energy Agency: Paris, France, 2022.
3. Adamo, A.; De La Hoz, J.; Martín, H.; Rubio, J.; Coronas, S. An Analysis of the Development of the Cogeneration Sector in Spain: A Comprehensive Review of the Period 1980–2020 from a Regulatory Perspective. *Energies* **2024**, *17*, 625. [CrossRef]
4. Armoo, E.A.; Mohammed, M.; Narra, S.; Beguedou, E.; Agyenim, F.B.; Kemausuor, F. Achieving Techno-Economic Feasibility for Hybrid Renewable Energy Systems through the Production of Energy and Alternative Fuels. *Energies* **2024**, *17*, 735. [CrossRef]
5. Wang, X.; Cui, C.; Pan, C.; Zhang, C.; Ren, H.; Ghias, A.M. A Deep Reinforcement Learning Control Strategy to Improve the Operating Flexibility of CHP Units under Variable Load Conditions. *Therm. Sci. Eng. Prog.* **2024**, *49*, 102482. [CrossRef]
6. Neacșa, A.; Panait, M.; Mureșan, J.D.; Voica, M.C.; Manta, O. The Energy Transition between Desideratum and Challenge: Are Cogeneration and Trigeneration the Best Solution? *Int. J. Environ. Res. Public Health* **2022**, *19*, 3039. [CrossRef] [PubMed]
7. Gu, Z.; He, S.; Li, X.; Sun, P.; Wu, J.; Hu, H.; Zhang, Q.; Jiang, J. Hundred-Watt Implantable TEG Module for Large-Scale Exhaust Gas Waste Heat Recovery. *Energies* **2024**, *17*, 665. [CrossRef]
8. Park, H. Locational Role Analysis of Energy Storage Systems Based on Optimal Capacity Needs and Operations under High Penetration of Renewable Energy. *Energies* **2024**, *17*, 743. [CrossRef]
9. Wang, J.; You, S.; Zong, Y.; Træholt, C.; Dong, Z.Y.; Zhou, Y. Flexibility of Combined Heat and Power Plants: A Review of Technologies and Operation Strategies. *Appl. Energy* **2019**, *252*, 113445. [CrossRef]
10. Figaj, R. Energy and Economic Sustainability of a Small-Scale Hybrid Renewable Energy System Powered by Biogas, Solar Energy, and Wind. *Energies* **2024**, *17*, 706. [CrossRef]
11. Yu, Y.X. Sodium/Potassium Intercalation on the Cu4S4 Nanosheet Accompanied by a Surface Phase Transition and Their Competition with Protons. *ACS Appl. Energy Mater.* **2023**, *6*, 10048–10060. [CrossRef]
12. Sun, F.; Zhao, X.; Chen, X.; Fu, L.; Liu, L. New Configurations of District Heating System Based on Natural Gas and Deep Geothermal Energy for Higher Energy Efficiency in Northern China. *Appl. Therm. Eng.* **2019**, *151*, 439–450. [CrossRef]
13. Amaris, C.; Miranda, B.; Balbis-Morejón, M. Experimental Thermal Performance and Modelling of a Waste Heat Recovery Unit in an Energy Cogeneration System. *Therm. Sci. Eng. Prog.* **2020**, *20*, 100684. [CrossRef]
14. Giordano, L.; Benedetti, M. A Methodology for the Identification and Characterization of Low-Temperature Waste Heat Sources and Sinks in Industrial Processes: Application in the Italian Dairy Sector. *Energies* **2022**, *15*, 155. [CrossRef]
15. Farshi, L.G.; Khalili, S. Thermoeconomic Analysis of a New Ejector Boosted Hybrid Heat Pump (EBHP) and Comparison with Three Conventional Types of Heat Pumps. *Energy* **2019**, *170*, 619–635. [CrossRef]
16. Abdelkareem, M.A.; Maghrabie, H.M.; Sayed, E.T.; Kais, E.C.A.; Abo-Khalil, A.G.; Radi, M.A.; Baroutaji, A.; Olabi, A. Heat Pipe-Based Waste Heat Recovery Systems: Background and Applications. *Therm. Sci. Eng. Prog.* **2022**, *29*, 101221. [CrossRef]
17. Nandhini, R.; Sivaprakash, B.; Rajamohan, N. Waste Heat Recovery at Low Temperature from Heat Pumps, Power Cycles and Integrated Systems—Review on System Performance and Environmental Perspectives. *Sustain. Energy Technol. Assess.* **2022**, *52*, 102214. [CrossRef]
18. Zhang, H.; Liu, Y.; Liu, X.; Duan, C. Energy and Exergy Analysis of a New Cogeneration System Based on an Organic Rankine Cycle and Absorption Heat Pump in the Coal-Fired Power Plant. *Energy Conv. Manag.* **2020**, *223*, 113293. [CrossRef]
19. Zhao, S.; Wang, W.; Ge, Z. Thermodynamic, Operational, and Techno-Economic Analysis of the Cascade Heating System with a Double-Unit. *Energy Conv. Manag.* **2020**, *226*, 113558. [CrossRef]
20. Chen, H.; Xiao, Y.; Xu, G.; Xu, J.; Yao, X.; Yang, Y. Energy-Saving Mechanism and Parametric Analysis of the High Back-Pressure Heating Process in a 300 MW Coal-Fired Combined Heat and Power Unit. *Appl. Therm. Eng.* **2019**, *149*, 829–840. [CrossRef]
21. Chen, C.; Ge, Z.; Zhang, Y. Study of Combined Heat and Power Plant Integration with Thermal Energy Storage for Operational Flexibility. *Appl. Therm. Eng.* **2023**, *219*, 119537. [CrossRef]
22. Wang, X.; Wu, Y.; Fu, L. Evaluation of Combined Heat and Power Plants with Electricity Regulation. *Appl. Therm. Eng.* **2023**, *227*, 120364. [CrossRef]
23. Zhang, Y.; Ge, Z.; Yang, Y.; Hao, J.; Xu, L.; Du, X.; Træholt, C. Carbon Reduction and Flexibility Enhancement of the CHP-based Cascade Heating System with Integrated Electric Heat Pump. *Energy Conv. Manag.* **2023**, *280*, 116801. [CrossRef]
24. Ahmed, F.; Chen, W. Investigation of Steam Ejector Parameters under Three Optimization Algorithm Using ANN. *Appl. Therm. Eng.* **2023**, *225*, 120205. [CrossRef]
25. Paul, S.; Kumar, P.; Rao, S.M. Thermodynamic Analysis on the Effect of Supercritical CO_2 Ejector in Cogeneration Cycle for Dairy Application. *Therm. Sci. Eng. Prog.* **2023**, *39*, 101729. [CrossRef]
26. Siddiqui, M.A.; Khaliq, A.; Kumar, R. Proposal and Analysis of a Novel Cooling-Power Cogeneration System Driven by the Exhaust Gas Heat of HCCI Engine Fuelled by Wet-Ethanol. *Energy* **2021**, *232*, 120954. [CrossRef]
27. Ifaei, P.; Safder, U.; Tayerani Charmchi, A.S.; Yoo, C. An Integrated Steam Jet Ejector Power Plant for Drought Adaptation Considering Water-Exergy Nexus in an Optimal Platform. *Energy Conv. Manag.* **2021**, *227*, 113622. [CrossRef]
28. Pang, J.; Ge, Z.; Zhang, Y.; Du, X. Comparative Designs and Optimizations of the Steam Ejector for a CHP System. *Appl. Therm. Eng.* **2023**, *226*, 120345. [CrossRef]
29. Liu, M.; Liu, M.; Wang, Y.; Chen, W.; Yan, J. Thermodynamic Optimization of Coal-Fired Combined Heat and Power (CHP) Systems Integrated with Steam Ejectors to Achieve Heat—Power Decoupling. *Energy* **2021**, *229*, 120707. [CrossRef]

30. Chen, H.; Wang, Y.; Li, J.; Xu, G.; Lei, J.; Liu, T. Thermodynamic Analysis and Economic Assessment of an Improved Geothermal Power System Integrated with a Biomass-Fired Cogeneration Plant. *Energy* **2022**, *240*, 122477. [CrossRef]
31. Cao, Y.; Dhahad, H.A.; Togun, H.; Haghghi, M.A.; Anqi, A.E.; Farouk, N.; Rosen, M.A. Seasonal Design and Multi-Objective Optimization of a Novel Biogas-Fueled Cogeneration Application. *Int. J. Hydrogen Energy* **2021**, *46*, 21822–21843. [CrossRef]
32. Fazeli, A.; Zandi, S.; Golbaten Mofrad, K.; Salehi, G.; Khoshgoftar Manesh, M.H.; Shirmohammadi, R. Comparative Thermoeconomic Optimization and Exergoenvironmental Analysis of an Ejector Refrigeration Cycle Integrated with a Cogeneration System Utilizing Waste Exhaust Heat Recovery. *Environ. Prog. Sustain. Energy* **2022**, *41*, e13875. [CrossRef]
33. Zhang, Y.; Xiong, N.; Ge, Z.; Zhang, Y.; Hao, J.; Yang, Z. A Novel Cascade Heating System for Waste Heat Recovery in the Combined Heat and Power Plant Integrating with the Steam Jet Pump. *Appl. Energy* **2020**, *278*, 115690. [CrossRef]
34. Liu, M.; Liu, M.; Chen, W.; Yan, J. Operational Flexibility and Operation Optimization of CHP Units Supplying Electricity and Two-Pressure Steam. *Energy* **2023**, *263*, 125988. [CrossRef]
35. Chen, W.; Zhang, S.; Ahmed, F.; Fan, J.; Chong, D.; Yan, J. Simulation Investigation on Performance of a Power—Water Cogeneration System Coupled with a Two-Stage Thermal Vapor Compressor. *Case Stud. Therm. Eng.* **2021**, *28*, 101435. [CrossRef]
36. Tan, Z.; Feng, X.; Wang, Y. Performance Comparison of Different Heat Pumps in Low-Temperature Waste Heat Recovery. *Renew. Sustain. Energy Rev.* **2021**, *152*, 111634. [CrossRef]
37. Zhao, S.; Ge, Z.; Sun, J.; Ding, Y.; Yang, Y. Comparative Study of Flexibility Enhancement Technologies for the Coal-Fired Combined Heat and Power Plant. *Energy Conv. Manag.* **2019**, *184*, 15–23. [CrossRef]
38. Li, Y.; An, H.; Li, W.; Zhang, S.; Jia, X.; Fu, L. Thermodynamic, Energy Consumption and Economic Analyses of the Novel Cogeneration Heating System Based on Condensed Waste Heat Recovery. *Energy Conv. Manag.* **2018**, *177*, 671–681. [CrossRef]
39. Ma, J.; Wu, Y.; Chen, X. A New Integration Scheme for CO_2 Capture in Low-Rank Coal Fired Power Plants with Energy Savings. *Appl. Therm. Eng.* **2023**, *228*, 120476. [CrossRef]

Disclaimer/Publisher's Note: The statements, opinions and data contained in all publications are solely those of the individual author(s) and contributor(s) and not of MDPI and/or the editor(s). MDPI and/or the editor(s) disclaim responsibility for any injury to people or property resulting from any ideas, methods, instructions or products referred to in the content.